Environmental Science & Technology

Article

pubs.acs.org/est

Hydroquinone and Quinone-Grafted Porous Carbons for Highly Selective CO_2 Capture from Flue Gases and Natural Gas Upgrading

Jun Wang,[†] Rajamani Krishna,[‡] Jiangfeng Yang,[§] and Shuguang Deng*[,†]

[†]Chemical & Materials Engineering Department, New Mexico State University, Las Cruces, New Mexico 88003, United States
[‡]Van't Hoff Institute for Molecular Sciences, University of Amsterdam, Science Park 904, 1098 XH Amsterdam, The Netherlands
[§]Research Institute of Special Chemicals, Taiyuan University of Technology, Taiyuan 030024, Shanxi, PR China

Supporting Information

ABSTRACT: Hydroquinone and quinone functional groups were grafted onto a hierarchical porous carbon framework via the Friedel–Crafts reaction to develop more efficient adsorbents for the selective capture and removal of carbon dioxide from flue gases and natural gas. The oxygen-doped porous carbons were characterized with scanning electron microscopy, transmission electron microscopy, X-ray powder diffraction, Fourier transform infrared spectroscopy, and Raman spectroscopy. CO_2, CH_4, and N_2 adsorption isotherms were measured and correlated with the Langmuir model. An ideal adsorbed solution theory (IAST) selectivity for the CO_2/N_2 separation of 26.5 (298 K, 1 atm) was obtained on the hydroquinone-grafted carbon, which is 58.7% higher than that of the pristine porous carbon, and a CO_2/CH_4 selectivity value of 4.6 (298 K, 1 atm) was obtained on the quinone-grafted carbon (OAC-2), which represents a 28.4% improvement over the pristine porous carbon. The highest CO_2 adsorption capacity on the oxygen-doped carbon adsorbents is 3.46 mmol g^{-1} at 298 K and 1 atm. In addition, transient breakthrough simulations for $CO_2/CH_4/N_2$ mixture separation were conducted to demonstrate the good separation performance of the oxygen-doped carbons in fixed bed adsorbers. Combining excellent adsorption separation properties and low heats of adsorption, the oxygen-doped carbons developed in this work appear to be very promising for flue gas treatment and natural gas upgrading.

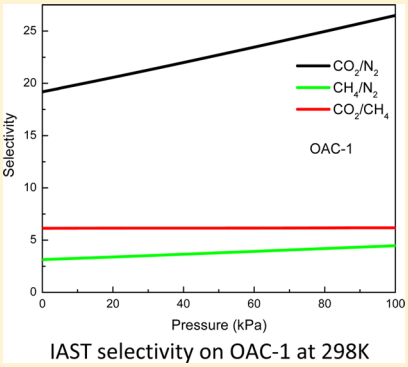

IAST selectivity on OAC-1 at 298K

INTRODUCTION

The continuously increasing CO_2 level in the atmosphere has attracted the world's attention during last a few decades due to its potential environment damage. This motivates people to find various ways to capture CO_2, such as sequestrate carbon in the soil,[1] porous adsorbents,[2,3] and ocean fertilization.[4] Although a range of methods to capture and store CO_2 has been investigated and developed, the liquid amine doped adsorbents are still the primary industrial approach.[5,6] However, this technology is not perfect due to some inherent drawbacks, such as amine degradation, evaporative losses, and high regeneration energy costs.[7] Low-quality natural gas such as biogas and land fill gas consists predominantly of CH_4 and has some impurities. The presence of CO_2 and N_2 in natural gas could dramatically reduce the heating value and cause pipeline corrosion. Thus, separating impurities from CH_4 is required.

Porous materials have been proposed as good alternative adsorbents for the selective removal of carbon dioxide from flue gases and natural gas because they possess good chemical resistance and energy-efficient regeneration. Porous materials such as metal–organic frameworks (MOFs),[8,9] hyper-cross-linked polymers (HCPs),[10,11] covalent organic frameworks (COFs),[12] and amine-based cellulose[13] are being considered in industrial applications and are at various stages of development. Among those porous materials, activated carbons are one of the most studied materials. Activated carbons have been used for many purposes such as wastewater treatment,[14] battery electrodes,[15] and supercapacitors.[16] Activated carbon continues to be a particularly intriguing alternative adsorbent because of its ease of synthesis, high CO_2 adsorption capacity, excellent selectivity and stability, and ease of regeneration.[17−19] To improve CO_2 capacity, we can either optimize the pore architecture by changing the synthetic parameters or modifying the surface properties through adding functional groups.[20,21] Secilla et al. demonstrated the importance of both microporosity and the presence of polar, basic functional groups in improving CO_2 adsorption.[22]

To improve the CO_2 adsorption capacity and selectivity, incorporating functional groups into carbon materials is very important because they could enhance the affinity between adsorbate molecules and adsorbents. The common way is to introduce nitrogen-containing groups into the framework of activated carbon, due to its significant ability in improving interaction force. For example, Mahurin et al. demonstrated that an amidoxime-modified porous carbon displayed a CO_2 capacity of 4.97 mmol g^{-1} at 273 K and 1 atm, and enhanced CO_2/N_2 selectivity.[23] Chandra et al. reported an N-doped

Received: April 2, 2015
Revised: June 11, 2015
Accepted: June 26, 2015
Published: June 26, 2015

DOI: 10.1021/acs.est.5b01652
Environ. Sci. Technol. 2015, 49, 9364−9373

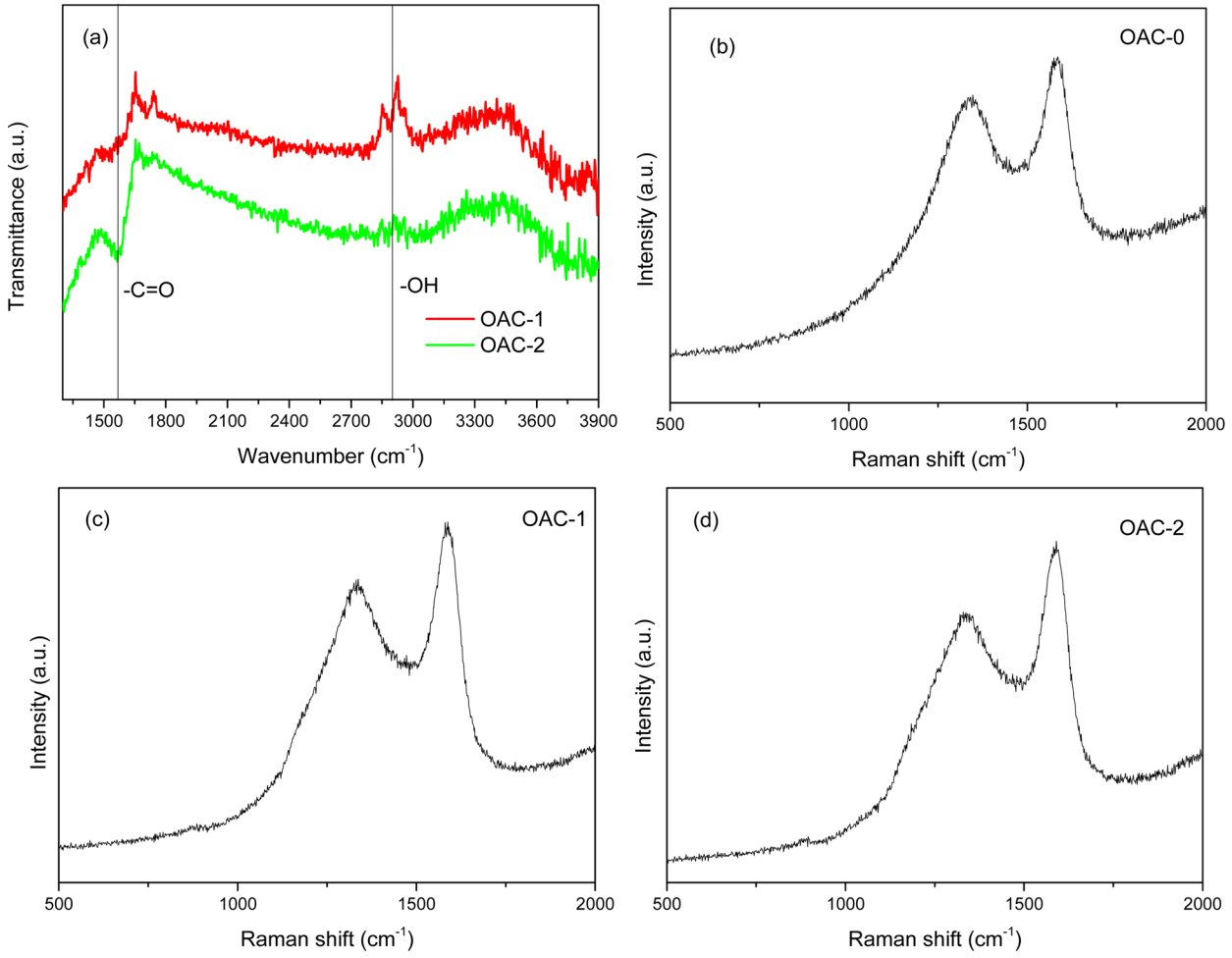

Figure 1. (a) FTIR spectra, (b) Raman pattern of OAC-0, (c) Raman pattern of OAC-1, and (d) Raman pattern of OAC-2.

carbon produced by the chemical activation of polypyrrole, which has a CO_2 capacity of 4.3 mmol g^{-1} at 298 K and 1 atm and good CO_2/N_2 selectivty (approximately 34).[24] Although integrating nitrogen groups is the most studied method, other functional groups have been investigated recently; for example, Seema et al. reported on S-doped carbon and discovered a CO_2 capacity of 4.3 mmol g^{-1} at 298 K and 1 atm.[25] Plaza et al. demonstrated the impact of oxidation on the CO_2 capacity of phenolic resin carbon and observed an enhancement in uptake in the oxidized carbon.[26] Thus, doping heteroatoms is an alternative method for enhancing CO_2 capture via electrostatics interactions. In 2013, Isikli et al. reported the influence of quinone grafting on carbon porous structure and supercapacitor performance.[27] The primary motivation of this work is to create porous carbon modified by hydroquinone and quinone groups and investigate the impact of the oxygen-containing groups on CO_2 adsorption and on the selective adsorption of gas mixture pairs containing CO_2.

MATERIALS AND METHODS

Synthesis of OAC Material. Furan, dichloromethane (DCE), formaldehyde, anhydrous iron(III) chloride ($FeCl_3$), methanol, 1,4,-benzoquinone (*p*-BQ), 2,3-dicloro-5,6-dicyano-1,4-benzoquinone (DDQ), and zinc chloride ($ZnCl_2$) were purchased from Sigma-Aldrich. Hydrochloric acid (HCl) was purchased from Fisher Scientific. All chemicals were used as received without any further purification. To synthesize polyfuran (PF), we dispersed 3 g of furan in 50 mL dichloromethane (DCE) at room temperature using sonication. A total of 8 g of $FeCl_3$ dissolved in 50 mL DCE was added to this solution. The resulting solution was stirred and allowed to polymerize for 24 h at room temperature. After polymerization, the precipitate was washed and dried at 80 °C for 24 h in a vacuum. The calcination of OAC-0 was carried out using a 1:1 ratio of PF and zinc chloride at 600 °C for 1 h under N_2 atmosphere at 600 °C with a heating rate of 3 °C/min. After activation, the product was washed with HCl solution until a neutral pH was observed and then washed with DI water and dried under a vacuum at 80 °C for 24 h. Modified carbons were prepared following the reported process.[27] OAC-1 was prepared by a typical Friedel−Crafts reaction: OAC-0, *p*-BQ, $FeCl_3$, and DCE were mixed into a round-bottom flask. The mixture was stirred vigorously at room temperature under nitrogen protection overnight. Part of the precipitation was collected by filtration, washed, dried under a vacuum at 80 °C for 24 h, and denoted as OAC-1. We then added DDQ into the mixture and stirred it for 3 h to complete the oxidation of the hydroquinone intermediate at a room temperature. The final product was washed and dried under a vacuum at 80 °C for 24 h and denoted as OAC-2.

Material Characterization. The XRD pattern was recorded using a Rigaku Miniflex-II X-ray diffractometer with Cu Kα (λ = 1.5406 Å) radiation, a 30 kV/15 mA current, and a kβ-filter. Fourier transformed infrared (FT-IR) spectra were

DOI: 10.1021/acs.est.5b01652
Environ. Sci. Technol. 2015, 49, 9364−9373

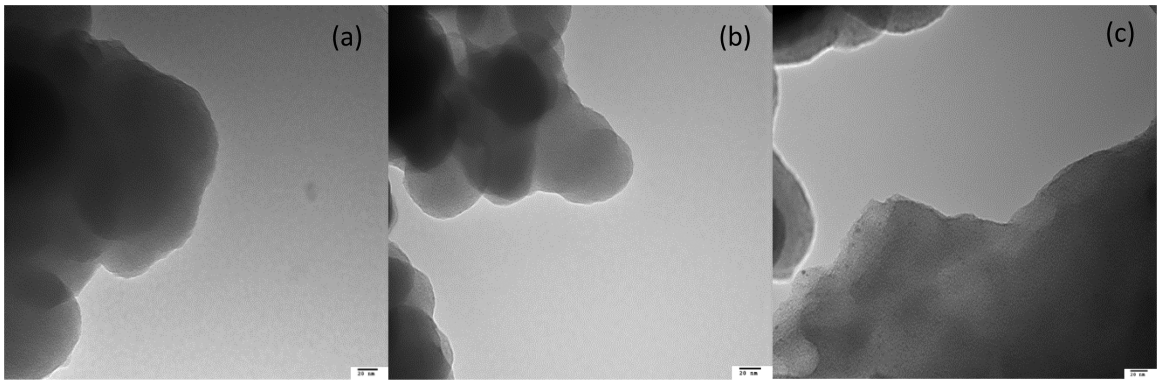

Figure 2. TEM images of (a) OAC-0, (b) OAC-1, and (c) OAC-2.

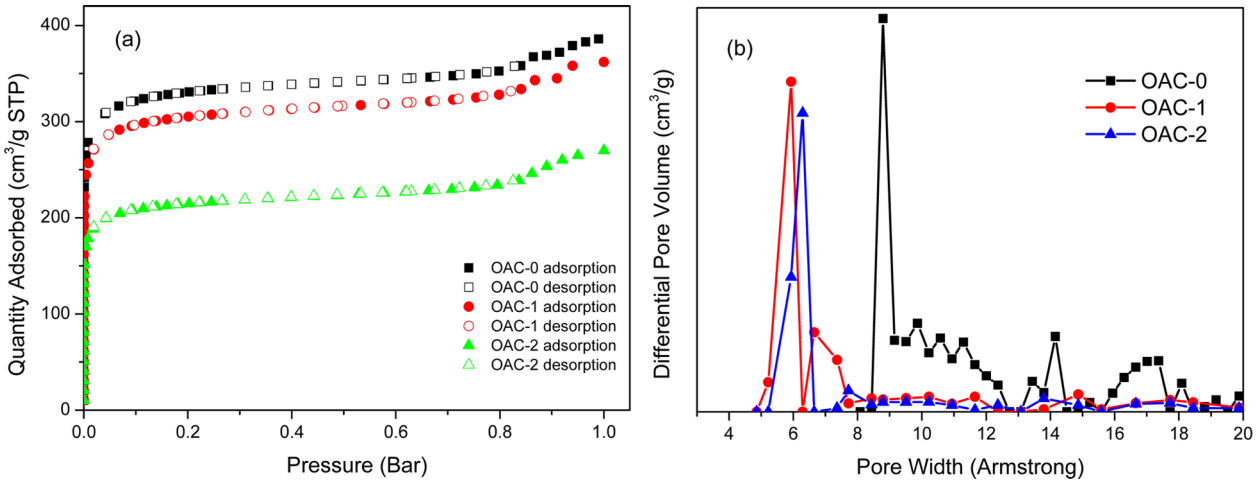

Figure 3. (a) N_2 adsorption isotherms and (b) pore size distributions for OACs.

Table 1. Textual Properties of Oxygen-Doped Porous Carbons

sample	S_{BET} [a] (m^2/g)	S_{Lang} [b] (m^2/g)	V_p [c] (cm^3/g)	S_{micro} [d] (m^2/g)	V_{micro} [d] (m^3/g)	D_{pore} [e] (nm)	oxygen content[f] (wt %)
OAC-0	1006	1567	0.57	1304	0.51	1.1	1.57
OAC-1	925	1461	0.53	1156	0.45	0.6	7.51
OAC-2	653	1046	0.38	854	0.34	0.7	3.38

[a]The specific surface area was determined by the BET equation (p/p_0 = 0.05−0.3). [b]The specific surface area was determined by the Langmuir equation (p/p_0 = 0.05−0.98). [c]Total pore volume at p/p_0 = 0.98. [d]The micropore volume and micropore surface area were estimated as d < 2 nm using the equilibrium model for slit pores. [e]The maxima of the pore size distribution was calculated by the NLDFT method. [f]The oxygen content was determined by energy-dispersive X-ray (EDS) spectroscopy.

recorded with a PerkinElmer FTIR. Scanning electron microscopy (SEM) images and readings of the oxygen content of the materials were taken using an SEM S-3400NII equipped with energy-dispersive X-ray analysis. Transmission electron microscopy (TEM) images were taken with a Hitachi H-7650. Raman spectra were collected using a Reinshaw Raman microscope with a 632.8 nm (1.96 eV) laser excitation.

Adsorption Measurements. The pure component adsorption isotherms of CO_2, CH_4, and N_2 at three temperatures (273, 298, and 323 K) and gas pressure up to 800 mmHg were measured volumetrically in the Micromeritics ASAP 2020 adsorption apparatus. The degassing procedure was repeated in all samples before measurements at 180 °C for 24 h. The BET (Brunauer−Emmett−Teller) surface area was calculated between 0.05 and 0.3 relative pressure, and pore size distributions were calculated using NLDFT (nonlocal density functional theory) from N_2 adsorption−desorption isotherms measured at 77K.

RESULTS AND DISCUSSION

Material Synthesis and Characterization. The FTIR spectra of OAC-1 and OAC-2 are shown in Figure 1a. After the synthetic modification, the adsorption band of C═O becomes more intense at 1612 cm^{-1}, and the adsorption band of OH at 2896 cm^{-1} is almost invisible on OAC-2, indicating that the conversion from C−OH to C═O is completed. Also, the FTIR pattern of OAC-2 does not show additional adsorption at 2200 cm^{-1}, allowing us to determine that the washing process after the grafting is effective. Because the stretching bond at this position could be attributed to the nitrile group (CN) present in DDQ or its reduced form,[27] the defective nature in high-temperature-activated carbon can be confirmed by Raman spectra (Figure 1 b−d). The Raman patterns evidence that two peaks with broad bands at around 1358 and 1588 cm^{-1} can be found, which correspond to the D and G bands, respectively. The D band corresponds to the breath modes of the rings or κ-

DOI: 10.1021/acs.est.5b01652
Environ. Sci. Technol. 2015, 49, 9364−9373

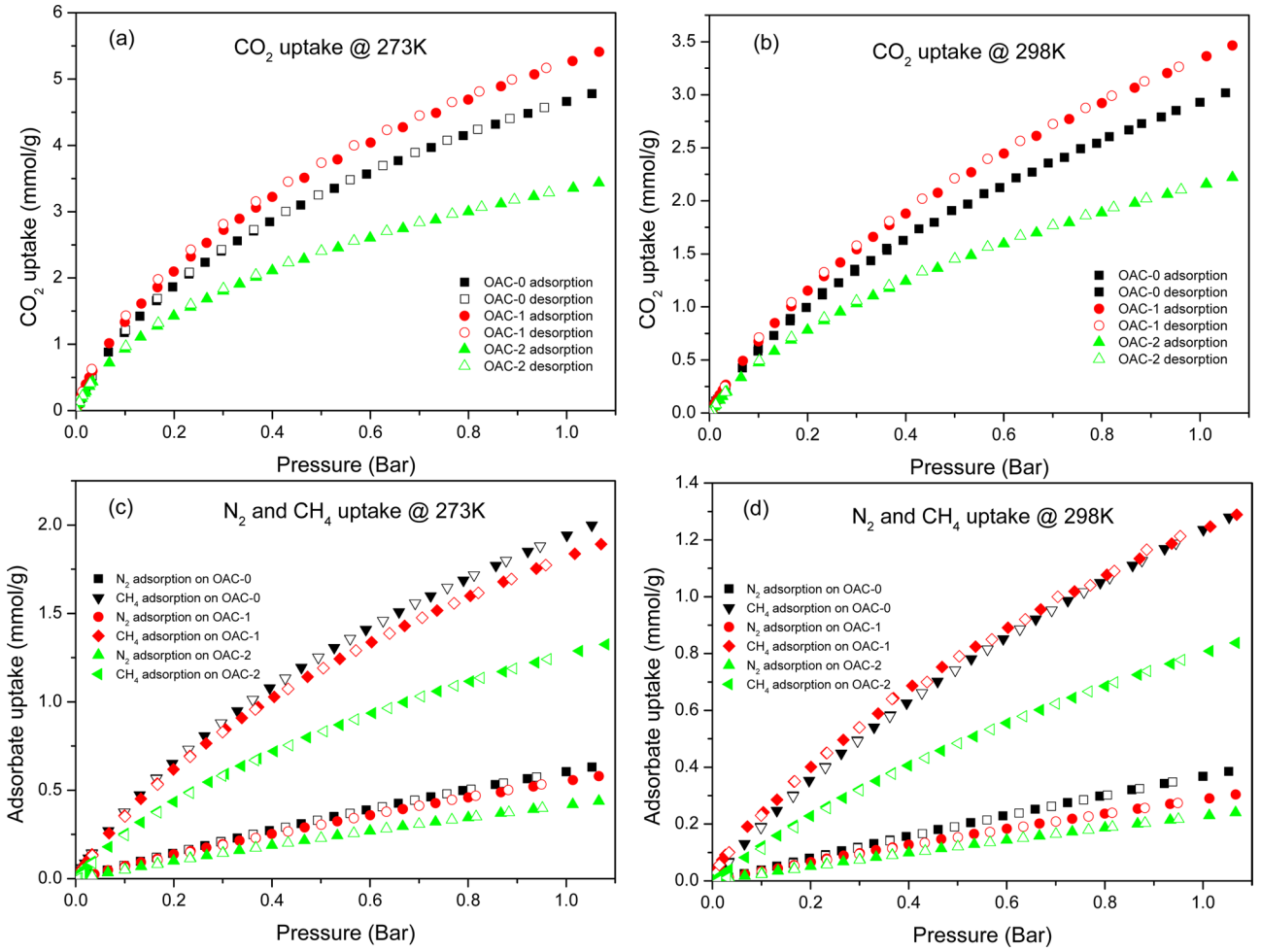

Figure 4. (a) CO_2 adsorption at 273 K, (b) CO_2 adsorption at 298 K, (c) N_2 and CH_4 adsorption at 273 K, and (d) N_2 and CH_4 adsorption at 298 K of OAC-0, OAC-1, and OAC-2.

Table 2. Adsorption Properties of Oxygen-Doped Porous Carbons

	CO_2 adsorption (1 bar, mmol/g)		CH_4 adsorption (1 bar, mmol/g)		N_2 adsorption (1 bar, mmol/g)	
sample	0 °C	25 °C	0 °C	25 °C	0 °C	25 °C
OAC-0	4.78	3.02	2.00	1.28	0.63	0.39
OAC-1	5.41	3.46	1.89	1.29	0.58	0.30
OAC-2	3.43	2.22	1.32	0.84	0.44	0.24

point phonons of A1g symmetry, while the G band represents the in-plane bond-stretching motion of the pairs of C sp2 atoms (the E2g phonons).[28,29] The intensity ratio between D and G bands (I_G/I_D) could exactly reflect the degree of graphitization in carbon materials. The ratio is 0.58, 0.55, and 0.53 for OAC-0, OAC-1, and OAC-2, respectively. The decreasing values indicate that OAC-1 and OAC-2 possess the more defective nature and lower degree of graphitization. This could be attributed to a disordered structure caused by grafting modifications. The XRD patterns are shown in Figure S1 in the Supporting Information; the three labeled peaks at 2θ values of 32, 34, and 36° could be contributed from the Zn species. The carbon precursors were carbonized at 873 K, while the Zn metal boiling point is about 1181 K; thus, the Zn metal could not be vaporized completely under the carbonization conditions. The empirical parameter (R) was used to evaluated the degree of graphitization, which is defined as the ratio of height of the (0 0 2) Bragg peak to the background.[30,31] Therefore, the graphitization of OAC-1 and OAC-2 is higher than that of OAC-0 due to its more apparent (0 0 2) peak.

To establish the impact of the decorated groups on the pore structure, we acquired SEM images for all OACs (Figure S2 in the Supporting Information). A comparison of the microscopy images shows that the addition of the decorated groups does not alter the primary structure of the carbon. TEM images are shown in Figure 2; the micropores are randomly and uniformly distributed on all OACs. The texture properties of the OACs were further examined using nitrogen adsorption isotherms at 77 K. Figure 3 summarizes all of the isotherms and their corresponding pore size distribution using the NLDFT method. It is clear that all isotherms displayed a typical type I shape according to IUPAC classification.[32] The steep adsorption at the low pressure indicates that all of the pores are micropores (<2 nm). As shown in Table 1, which includes the specific surface areas and pore volumes for each OAC, the BET surface area is 1006, 925, and 653 $m^2\ g^{-1}$ for OAC-0, OAC-1, and OAC-2, respectively; the pore volume is 0.57, 0.53, and 0.38 $cm^3\ g^{-1}$ for OAC-0, OAC-1, and OAC-2, respectively. We noted that both the specific surface area and the pore volume significantly decrease after grafting functional groups because the addition groups block partial pore volume. Thus, the pore size is also reduced from 1.1 to 0.6 nm.

DOI: 10.1021/acs.est.5b01652
Environ. Sci. Technol. 2015, 49, 9364−9373

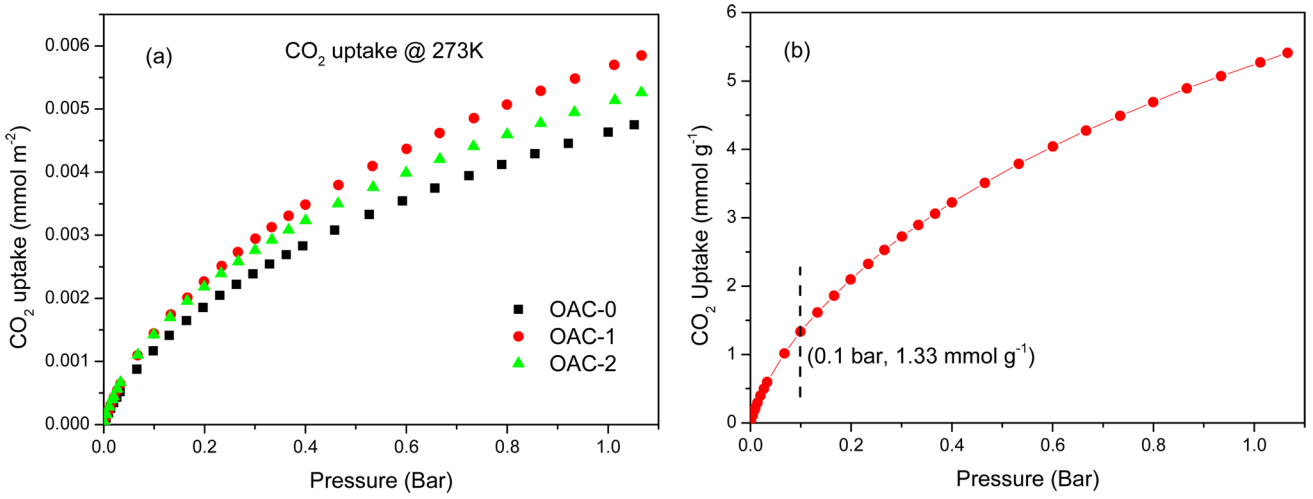

Figure 5. (a) CO_2 adsorption at 273 K of OACs normalized with respect to the surface areas. (b) CO_2 adsorption of OAC-1 at 273 K.

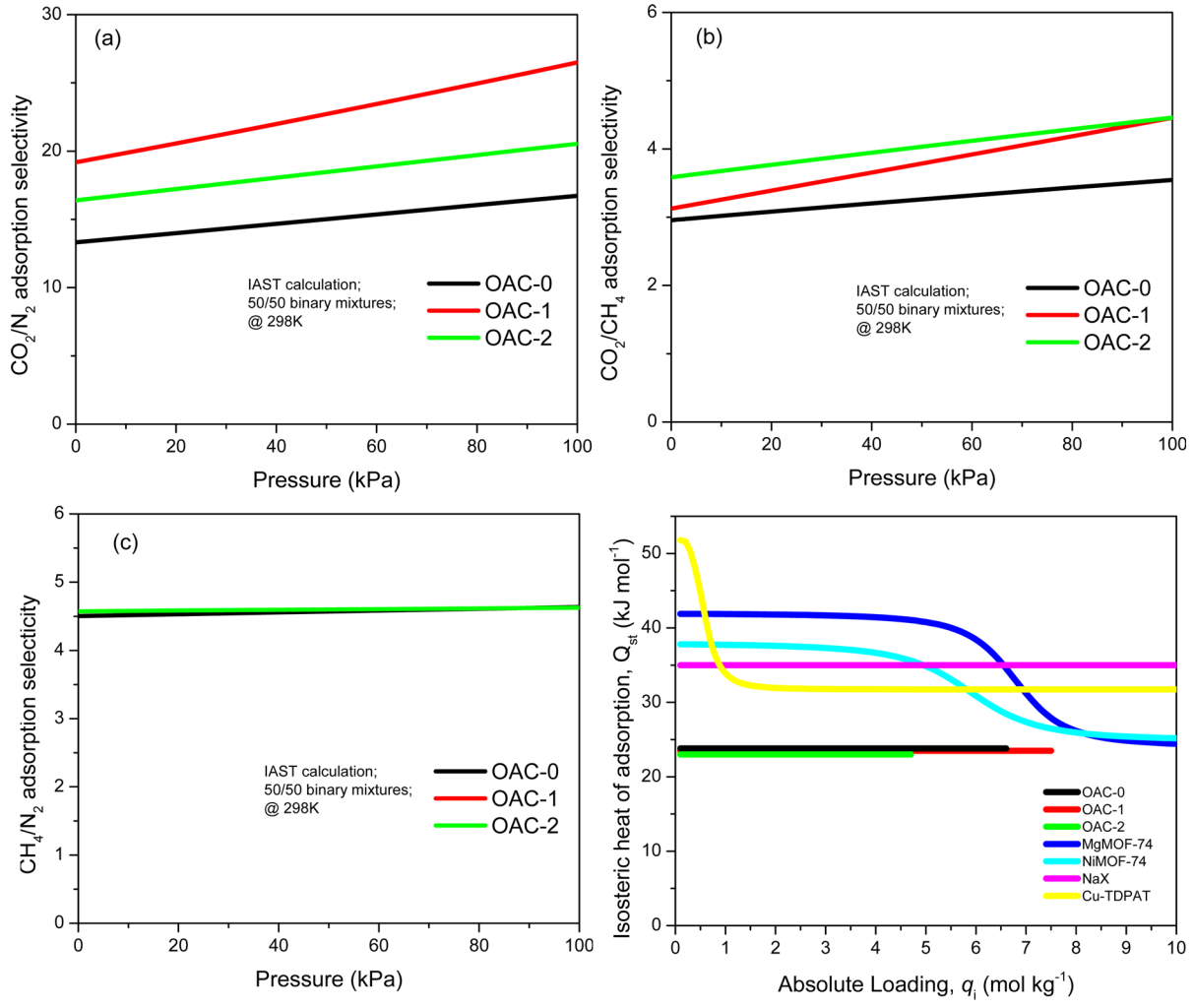

Figure 6. IAST-predicted adsorption selectivities for equimolar binary mixtures of (a) CO_2/CH_4, (b) CH_4/N_2, and (c) CO_2/N_2. (d) Isosteric heats of adsorption for CO_2 on the OACs, MgMOF-74, NiMOF-74, Cu-TDPA, and NaX.

Adsorption Isotherms of CO_2, CH_4, and N_2. The adsorption isotherms of CO_2, N_2, and CH_4 were measured at 273, 298, and 323 K and the pressure measured up to 1 bar, as shown in Figure 4, Table 2 , and Figures S3 and S4 in the Supporting Information. All isotherms showed excellent reversibility without any hysteresis, indicating that a vacuum can remove all of the adsorbate molecules during the desorption process. Thus, OACs can be easily regenerated without any other heat energy input. All adsorption isotherms were fitted by the Langmuir−Freundlich model. The

DOI: 10.1021/acs.est.5b01652
Environ. Sci. Technol. 2015, 49, 9364−9373

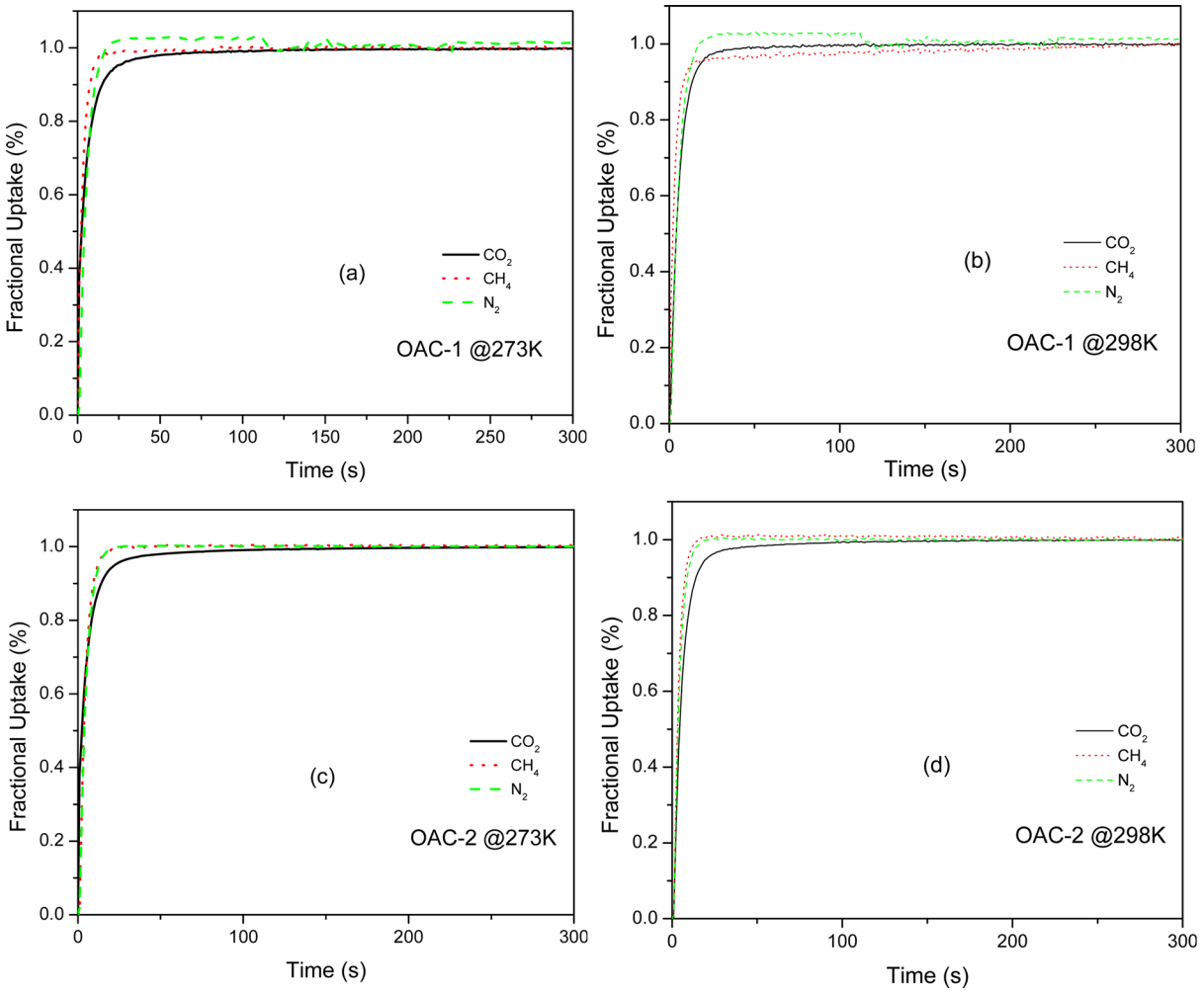

Figure 7. CO_2, CH_4, and N_2 fractional uptake on (a) OAC-1 at 273 K, (b) OAC-1 at 298 K, (c) OAC-2 at 273 K, and (d) OAC-2 at 298 K.

Table 3. Summary of Diffusion Time Constants of CO_2, CH_4, and N_2 on the Oxygen-Doped Porous Carbons at 273 and 298 K

sample	T (k)	CO_2 D_c/r_c^2 (10^{-3} s^{-1})	CH_4 D_c/r_c^2 (10^{-2} s^{-1})	N_2 D_c/r_c^2 (10^{-3} s^{-1})
OAC-1	273	7.2	1.2	6.2
	298	7.3	1.3	6.2
OAC-2	273	7.7	7.1	6.2
	298	7.8	8.2	7.3

calculation detail and parameters are summarized in Tables S1, S2, and S3 in the Supporting Information. It is clear that OACs adsorb CO_2 to a much greater degree than N_2 and CH_4 because of its higher quadrupole moment and polarizability. CH_4 is preferentially adsorbed over N_2 because the polarizability of CH_4 is higher than that of N_2.[33,34] The highest CO_2 capacity was obtained by OAC-1, measured to be 5.41 and 3.46 mmol g^{-1} at 273 and 298 K, respectively. This result is superior to other recently reported activated carbons.[7,35,36] Compared with that of the original material (OAC-0), the CO_2 capacity of OAC-1 increased, whereas the capacity of OAC-2 decreased from 4.78 to 3.43 mmol g^{-1} at 1 bar and 273 K. To clarify the effect of oxygen-containing groups decorated on CO_2 uptake capacity, we normalized the CO_2 uptake values with respect to the surface areas (Figure 5a), which clearly showed the enhancement of CO_2 uptake with an increase of O content. Furthermore, the extremely high CO_2 uptake (1.33 mmol g^{-1} at 0.1 bar and 273 K) for OAC-1 confirms the stronger interaction of CO_2 molecules with more O-decorated carbon framework at low pressures. It is noteworthy that the partial pressure of CO_2 in flue gas is approximately 0.1−0.15 bar.

IAST Selectivities and Interaction Energy. The selectivity of the preferential adsorption of component 1 over component 2 in a mixture containing both, perhaps in the presence of other components as well, can be formally defined as

$$S_{ads} = \frac{q_1/q_2}{p_1/p_2}$$

In the above equation, q_1 and q_2 are the absolute component loadings of the adsorbed phase in the mixture. These component loadings are also termed the "uptake capacities". In all of the calculations presented below, the calculations of q_1 and q_2 are based on the use of the ideal adsorbed solution theory of Myers and Prausnitz.[37] The accuracy of the IAST calculations for the estimation of the component loadings for several binary mixtures in a wide variety of zeolites and MOFs has been established by comparison with configurational-bias Monte Carlo (CBMC) simulations of mixture adsorption.[38−40] Further details are provided in the Supporting Information. The selectivities of all equimolar binary combination of CO_2,

DOI: 10.1021/acs.est.5b01652
Environ. Sci. Technol. 2015, 49, 9364−9373

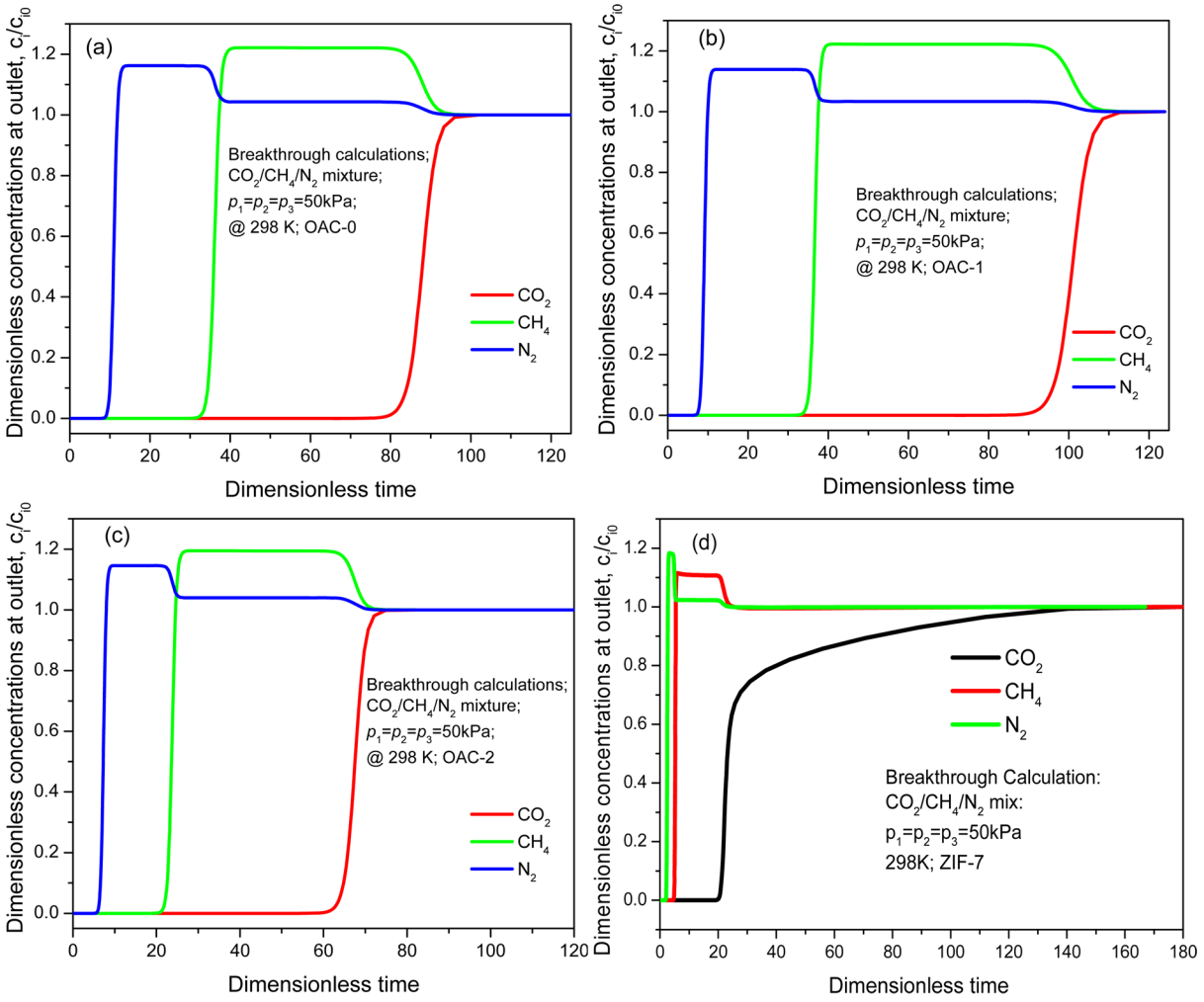

Figure 8. Breakthrough simulation data of (a) OAC-0, (b) OAC-1, (c) OAC-2, and (d) ZIF-7 at 298 K and 1 bar for an equimolar $CO_2/CH_4/N_2$ mixture (c_i, concentration of outlet gas; c_0, concentration of inlet gas).

CH_4, and N_2 at 298 K are present in Figure 6a–c. For CO_2/N_2 mixtures, the highest adsorption selectivities are obtained by the OAC-1 of 26.5 at 100 kPa, which is significantly higher than that of other adsorbents such as ordered mesoporous carbon (approximately 11.33),[41] MIL-47(V) (approximately 9),[42] and N-doped hierarchical carbons (approximately 8.4)[43] at 298 K. OAC-2 displayed the highest CO_2/CH_4 selectivity of 4.5 at 298 K and 100 kPa; these values are comparable to those of most existing adsorbents at the same condition, such as silicalite-1 (approximately 2.6),[44] SBA-15 (approximately 5.5),[45] and MCM-41 (approximately 5.5).[46] Modified activated carbons show higher CO_2/N_2 and CO_2/CH_4 selectivities due to their fine pore size and functional groups doping. It is worth noting that the CO_2/N_2 and CO_2/CH_4 selectivities are still increasing in high pressure because N_2 and CH_4 nearly reach their saturation capacities at 100 kPa, whereas the CO_2 loading is still far from saturation. Therefore, OACs will perform better in high pressure, which is easy to complete in industrial applications. For CH_4/N_2 gas mixtures, the adsorption selectivities of OACs are almost identical. At 298 K and 100 kPa, a CH_4/N_2 selectivity of 4.6 was obtained, which is higher than IRMOF-1 (approximately 2)[47] and ZIF-69 (approximately 3).[48] Those comparisons indicate that OACs are promising adsorbents in the selective adsorption of flue gases and natural gas processing.

The isosteric heats of adsorption for the OACs were accomplished by using adsorption isotherms at 273, 298, and 323 K. Isosteric heat of adsorption is a value with which to directly explore the interaction strength of adsorbates and adsorbents and further elucidate the origin of the enhanced selectivity. The values of Q_{st} for CO_2, CH_4, and N_2 are provided in Table S4 in the Supporting Information. Figure 6d presents a comparison of the isosteric heats of adsorption of CO_2 in OAC-0, OAC-1, and OAC-2 with data from other published literature for NaX zeolite,[49] MgMOF-74,[49] Cu-TDPAT,[50] and NiMOF-74.[51,52] This implies that the cost of regeneration for OACs will be significantly lower than that of other materials. This is an important advantage in favor of OACs when applied in industry. We noted that the Q_{st} for the three OACs are all mostly the same. The modified activated carbons are supposed to present higher values of adsorption heat; however, the value is not singly determined by decorated groups but also by the specific surface area and pore structure. The impact of the decreased specific area on OAC-1 and OAC-2 may offset the impact of oxygen doping.

Adsorption Kinetics. The adsorption kinetics data of CO_2, CH_4, and N_2 on the OACs were measured at three temperatures (273, 298, and 323 K) and low pressure (approximately 10 mmHg). The fractional uptake curves are presented in Figure 7 and Figure S5 in the Supporting

DOI: 10.1021/acs.est.5b01652
Environ. Sci. Technol. 2015, 49, 9364–9373

Information. At 298 K, CO_2 reaches equilibrium in 50 and 60 s for OAC-1 and OAC-2, respectively, whereas CH_4 and N_2 reach equilibrium in 18 and 15 s for OAC-1 and OAC-2, respectively. In addition, doing so took slightly less time at a higher temperature for each gas.

The diffusion time constants (D_c/r_c^2, s^{-1}) can be extracted by fitting the fractional uptake curve with the following micropore diffusion model.[53,54] This model assumes the mass transfer resistance for gas adsorption is controlled by the intracrystalline diffusion. When the fractional uptake is less than 0.85, the curve could be correlated by

$$\frac{m_t}{m_\infty} \approx \frac{6}{\sqrt{\pi}}\sqrt{\frac{D_c t}{r_c^2}} - 3\frac{D_c t}{r_c^2}$$

where m_t/m_∞ is the fractional adsorption uptake, D_c (m^2/s) is the intracrystalline diffusivity of gas molecules in porous media, r_c (m) is the crystal radius, and t (s) is the time. The diffusion time constants of the three gases extracted from the kinetic profiles at three temperatures are summarized in Table 3 and in Table S5 in the Supporting Information. It can be observed from Table 3 that CO_2 and N_2 are almost unable to be kinetically separated, and the kinetic selectivities of CO_2/CH_4 and CH_4/N_2 are less than 2. This implies that an efficient kinetic-based adsorption separation is difficult to achieve on the OACs. This is because the pore size is still too large compared to the kinetic diameters of the adsorbates, and the interaction force is not strong enough to hold one adsorbate for a longer time.

Transient Breakthrough Simulations. Separations using porous adsorbents are usually conducted in the fixed bed units; in such cases, the separation performance is dictated by a combination of adsorption selectivity and uptake capacity. For a proper evaluation of the performance of fixed bed adsorbers, it is necessary to carry out transient breakthrough simulations as described in the literature.[55,56] We therefore performed transient breakthrough simulations for the separation of $CO_2/CH_4/N_2$ gas mixtures on OACs, as shown in Figure 8. The methodology details and movies using the adsorption cycle isotherm fits are provided in the Supporting Information; the methodology used has been verified to be of good accuracy.[5557] For all OACs, the sequence of breakthroughs is N_2, CH_4, and CO_2. This is dictated by the hierarchy of adsorption strengths. CO_2 molecules are strongly adsorbed by OACs, which elute last in the sequence. The longest retention time was obtained on OAC-1, and this material has the best separation performance due to it having the highest CO_2 capacity and highest CO_2/N_2 and CO_2/CH_4 adsorption selectivities. We noted that there is a time interval in which we can get pure CH_4 or N_2 using OACs. We compare OACs with ZIF-7 using a breakthrough simulation under the same condition. The CO_2 and CH_4 adsorption data of ZIF-7 are from one recently published paper by our group,[58] and the N_2 adsorption is obtained from a U.S. patent.[59] It is clear that the time interval of $CO_2/CH_4/N_2$ pairs on ZIF-7 is much shorter than that of OACs. This implies OACs are more efficient and promising than ZIF-7 in industrial applications.

■ ASSOCIATED CONTENT

Supporting Information

Figures showing the XRD patterns of OACs; representative SEM images of materials showing pore structure; CO_2, CH_4, and N_2 adsorption and fractional uptake; and a shematic of the breakthrough apparatus. Tables showing the 1-site Langmuir parameters for the adsorption of CO_2, CH_4, and N_2; isoteric heats; and a summary of diffusion time constants. Additional details on IAST calculations, the isoteric heat of adsorption, simulation methodology for transient breakthrough in fixed bed adsorbers, notations, and references. Movie showing the adsorption cycle isotherm fit. The Supporting Information is available free of charge on the ACS Publications website at DOI: 10.1021/acs.est.5b01652.

■ AUTHOR INFORMATION

Corresponding Author

*Tel: +1-575-646-4346. Fax: +1-575-646-7706. E-mail: sdeng@nmsu.edu.

Notes

The authors declare no competing financial interest.

■ ACKNOWLEDGMENTS

This project was partially supported by the U.S. National Aeronautics and Space Administration (New Mexico Space Grant), the U.S. National Science Foundation (EEC 1028968), and the New Mexico State University Office of Vice President for Research (GREG awards for J.W. and X.W.). J.Y. acknowledges the Taiyuan University of Technology for supporting his visit to New Mexico State University.

■ REFERENCES

(1) Yao, Y.; Gao, B.; Fang, J.; Zhang, M.; Chen, H.; Zhou, Y.; et al. Characterization and environmental applications of clay−biochar composites. *Chem. Eng. J.* **2014**, *242* (0), 136−43.

(2) Yuan, B.; Wu, X. F.; Chen, Y. X.; Huang, J. H.; Luo, H. M.; Deng, S. G. Adsorption of CO2, CH4, and N-2 on Ordered Mesoporous Carbon: Approach for Greenhouse Gases Capture and Biogas Upgrading. *Environ. Sci. Technol.* **2013**, *47* (10), 5474−80.

(3) Yang, M.; Song, Y.; Jiang, L.; Zhu, N.; Liu, Y.; Zhao, Y.; et al. CO2 Hydrate Formation and Dissociation in Cooled Porous Media: A Potential Technology for CO2 Capture and Storage. *Environ. Sci. Technol.* **2013**, *47* (17), 9739−46.

(4) Matear, R. J.; Elliott, B. Enhancement of oceanic uptake of anthropogenic CO2 by macronutrient fertilization. *J. Geophys. Res.* **2004**, *109* (C4), C04001.

(5) Rochelle, G. T. Amine Scrubbing for CO2 Capture. *Science* **2009**, *325* (5948), 1652−4.

(6) Kim, D. Y.; Lee, H. M.; Min, S. K.; Cho, Y.; Hwang, I. C.; Han, K.; et al. CO2 Capturing Mechanism in Aqueous Ammonia: NH3-Driven Decomposition-Recombination Pathway. *J. Phys. Chem. Lett.* **2011**, *2* (7), 689−94.

(7) Mahurin, S. M.; Górka, J.; Nelson, K. M.; Mayes, R. T.; Dai, S. Enhanced CO2/N2 selectivity in amidoxime-modified porous carbon. *Carbon* **2014**, *67* (0), 457−64.

(8) Saha, D.; Bao, Z.; Jia, F.; Deng, S. Adsorption of CO2, CH4, N2O, and N2 on MOF-5, MOF-177, and Zeolite 5A. *Environ. Sci. Technol.* **2010**, *44* (5), 1820−6.

(9) Sabouni, R.; Kazemian, H.; Rohani, S. Mathematical Modeling and Experimental Breakthrough Curves of Carbon Dioxide Adsorption on Metal Organic Framework CPM-5. *Environ. Sci. Technol.* **2013**, *47* (16), 9372−80.

(10) Wood, C. D.; Tan, B.; Trewin, A.; Su, F.; Rosseinsky, M. J.; Bradshaw, D.; et al. Microporous organic polymers for methane storage. *Adv. Mater.* **2008**, *20* (10), 1916.

(11) Wang, J.; Huang, J. H.; Wu, X. F.; Yuan, B.; Sun, Y. Q.; Zeng, Z. L.; Deng, S. G. Effect of nitrogen group on selective separation of CO2/N-2 in porous polystyrene. *Chem. Eng. J.* **2014**, *256*, 390−397.

(12) Choi, Y. J.; Choi, J. H.; Choi, K. M.; Kang, J. K. Covalent organic frameworks for extremely high reversible CO2 uptake capacity: a theoretical approach. *J. Mater. Chem.* **2011**, *21* (4), 1073−8.

DOI: 10.1021/acs.est.5b01652
Environ. Sci. Technol. 2015, 49, 9364−9373

(13) Gebald, C.; Wurzbacher, J. A.; Tingaut, P.; Zimmermann, T.; Steinfeld, A. Amine-Based Nanofibrillated Cellulose As Adsorbent for CO2 Capture from Air. *Environ. Sci. Technol.* **2011**, *45* (20), 9101−8.
(14) Liu, Y.; Liu, H.; Wang, C.; Hou, S.-X.; Yang, N. Sustainable Energy Recovery in Wastewater Treatment by Microbial Fuel Cells: Stable Power Generation with Nitrogen-doped Graphene Cathode. *Environ. Sci. Technol.* **2013**, *47* (23), 13889−95.
(15) Permana, A. D. C.; Nugroho, A.; Chung, K. Y.; Chang, W.; Kim, J. Template-free synthesis of hierarchical porous anatase TiO2 microspheres with carbon coating and their electrochemical properties. *Chem. Eng. J.* **2014**, *241* (0), 216−27.
(16) Wen, X.; Chen, X.; Tian, N.; Gong, J.; Liu, J.; Rümmeli, M. H.; et al. Nanosized Carbon Black Combined with Ni2O3 as "Universal" Catalysts for Synergistically Catalyzing Carbonization of Polyolefin Wastes to Synthesize Carbon Nanotubes and Application for Supercapacitors. *Environ. Sci. Technol.* **2014**, *48* (7), 4048−55.
(17) Seema, H.; Kemp, K. C.; Le, N. H.; Park, S.-W.; Chandra, V.; Lee, J. W.; et al. Highly selective CO2 capture by S-doped microporous carbon materials. *Carbon* **2014**, *66* (0), 320−6.
(18) Ben, T.; Li, Y. Q.; Zhu, L. K.; Zhang, D. L.; Cao, D. P.; Xiang, Z. H.; et al. Selective adsorption of carbon dioxide by carbonized porous aromatic framework (PAF). *Energy Environ. Sci.* **2012**, *5* (8), 8370−6.
(19) Duan, J. G.; Higuchi, M.; Horike, S.; Foo, M. L.; Rao, K. P.; Inubushi, Y.; et al. High CO2/CH4 and C-2 Hydrocarbons/CH4 Selectivity in a Chemically Robust Porous Coordination Polymer. *Adv. Funct. Mater.* **2013**, *23* (28), 3525−30.
(20) Wahby, A.; Ramos-Fernandez, J. M.; Martinez-Escandell, M.; Sepulveda-Escribano, A.; Silvestre-Albero, J.; Rodriguez-Reinoso, F. High-surface-area carbon molecular sieves for selective CO_2 adsorption. *ChemSusChem* **2010**, *3* (8), 974−81.
(21) Sevilla, M.; Fuertes, A. B. Sustainable porous carbons with a superior performance for CO2 capture. *Energy Environ. Sci.* **2011**, *4* (5), 1765−71.
(22) Sevilla, M.; Valle-Vigon, P.; Fuertes, A. B. N-doped polypyrrole-based porous carbons for CO2 capture. *Adv. Funct. Mater.* **2011**, *21* (14), 2781−7.
(23) Mahurin, S. M.; Górka, J.; Nelson, K. M.; Mayes, R. T.; Dai, S. Enhanced CO2/N2 selectivity in amidoxime-modified porous carbon. *Carbon* **2014**, *67* (0), 457−64.
(24) Chandra, V.; Yu, S. U.; Kim, S. H.; Yoon, Y. S.; Kim, D. Y.; Kwon, A. H.; et al. Highly selective CO2 capture on N-doped carbon produced by chemical activation of polypyrrole functionalized graphene sheets. *Chem. Commun.* **2012**, *48* (5), 735−7.
(25) Seema, H.; Kemp, K. C.; Le, N. H.; Park, S. W.; Chandra, V.; Lee, J. W.; et al. Highly selective CO2 capture by S-doped microporous carbon materials. *Carbon* **2014**, *66*, 320−6.
(26) Plaza, M. G.; Thurecht, K. J.; Pevida, C.; Rubiera, F.; Pis, J. J.; Snape, C. E.; et al. Influence of oxidation upon the CO2 capture performance of a phenolic-resin-derived carbon. *Fuel Process. Technol.* **2013**, *110*, 53−60.
(27) Isikli, S.; Lecea, M.; Ribagorda, M.; Carreño, M. C.; Díaz, R. Influence of quinone grafting via Friedel−Crafts reaction on carbon porous structure and supercapacitor performance. *Carbon* **2014**, *66* (0), 654−61.
(28) Cancado L. G., Pimenta M. A., Neves B. R. A., Dantas M. S. S., Jorio A.Influence of the atomic structure on the Raman spectra of graphite edges.*Phys. Rev. Lett.* **2004**; *93* (24).10.1103/PhysRevLett.93.247401
(29) Ferrari, A. C.; Robertson, J. Interpretation of Raman spectra of disordered and amorphous carbon. *Phys. Rev. B: Condens. Matter Mater. Phys.* **2000**, *61* (20), 14095−107.
(30) Liu, Y. H.; Xue, J. S.; Zheng, T.; Dahn, J. R. Mechanism of lithium insertion in hard carbons prepared by pyrolysis of epoxy resins. *Carbon* **1996**, *34* (2), 193−200.
(31) Qu, D. Y. Investigation of hydrogen physisorption active sites on the surface of porous carbonaceous materials. *Chem. - Eur. J.* **2008**, *14* (3), 1040−6.
(32) Sing, K. S. W.; Everett, D. H.; Haul, R. A. W.; Moscou, L.; Pierotti, R. A.; Rouquerol, J.; et al. Reporting Physisorption Data for Gas Solid Systems with Special Reference to the Determination of Surface-Area and Porosity (Recommendations 1984). *Pure Appl. Chem.* **1985**, *57* (4), 603−19.
(33) Bae, Y. S.; Farha, O. K.; Hupp, J. T.; Snurr, R. Q. Enhancement of CO2/N-2 selectivity in a metal-organic framework by cavity modification. *J. Mater. Chem.* **2009**, *19* (15), 2131−4.
(34) Harlick, P. J. E.; Tezel, F. H. Adsorption of carbon dioxide, methane and nitrogen: pure and binary mixture adsorption for ZSM-5 with SiO2/Al2O3 ratio of 280. *Sep. Purif. Technol.* **2003**, *33* (2), 199−210.
(35) Aijaz, A.; Fujiwara, N.; Xu, Q. From Metal−Organic Framework to Nitrogen-Decorated Nanoporous Carbons: High CO2 Uptake and Efficient Catalytic Oxygen Reduction. *J. Am. Chem. Soc.* **2014**, *136* (19), 6790−3.
(36) Liu, R-L; Ji, W-J; He, T.; Zhang, Z-Q; Zhang, J.; Dang, F.-Q. Fabrication of nitrogen-doped hierarchically porous carbons through a hybrid dual-template route for CO_2 capture and haemoperfusion. *Carbon* **2014**, *76*, 84−95.
(37) Myers, A. L.; Prausnitz, J. M. Thermodynamics of mixed gas adsorption. *AIChE J.* **1965**, *11*, 121−130.
(38) Krishna, R.; van Baten, J. M. Using molecular simulations for screening of zeolites for separation of CO2/CH4 mixtures. *Chem. Eng. J.* **2007**, *133*, 121−131.
(39) Krishna, R.; van Baten, J. M. In Silico Screening of Zeolite Membranes for CO2 Capture. *J. Membr. Sci.* **2010**, *360*, 323−333.
(40) Krishna, R.; van Baten, J. M. In silico screening of metal-organic frameworks in separation applications. *Phys. Chem. Chem. Phys.* **2011**, *13*, 10593−10616.
(41) Yuan, B.; Wu, X. F.; Chen, Y. X.; Huang, J. H.; Luo, H. M.; Deng, S. G. Adsorption of CO2, CH4, and N-2 on Ordered Mesoporous Carbon: Approach for Greenhouse Gases Capture and Biogas Upgrading. *Environ. Sci. Technol.* **2013**, *47* (10), 5474−80.
(42) Liu, B.; Smit, B. Comparative Molecular Simulation Study of CO2/N-2 and CH4/N-2 Separation in Zeolites and Metal-Organic Frameworks. *Langmuir* **2009**, *25* (10), 5918−26.
(43) Gutierrez, M. C.; Carriazo, D.; Ania, C. O.; Parra, J. B.; Ferrer, M. L.; del Monte, F. Deep eutectic solvents as both precursors and structure directing agents in the synthesis of nitrogen doped hierarchical carbons highly suitable for CO2 capture. *Energy Environ. Sci.* **2011**, *4* (9), 3535−44.
(44) Yang, J. F.; Li, J. M.; Wang, W.; Li, L. B.; Li, J. P. Adsorption of CO2, CH4, and N-2 on 8-, 10-, and 12-Membered Ring Hydrophobic Microporous High-Silica Zeolites: DDR, Silicalite-1, and Beta. *Ind. Eng. Chem. Res.* **2013**, *52* (50), 17856−64.
(45) Saini, V. K.; Andrade, M.; Pinto, M. L.; Carvalho, A. P.; Pires, J. How the adsorption properties get changed when going from SBA-15 to its CMK-3 carbon replica. *Sep. Purif. Technol.* **2010**, *75*, 366−376.
(46) Belmabkhout, Y.; Sayari, A. Adsorption of CO2 from dry gases on MCM-41 silica at ambient temperature and high pressure. 2: Adsorption of CO2/N2, CO2/CH4 and CO2/H2 binary mixtures. *Chem. Eng. Sci.* **2009**, *64*, 3729−3735.
(47) Pires, J.; Saini, V. K.; Pinto, M. L. Studies on selective adsorption of biogas components on pillared clays: Approach for biogas improvement. *Environ. Sci. Technol.* **2008**, *42*, 8727−8732.
(48) Reyes, S. C.; Ni, Z.; Paur, C. S.; Kortunov, P.; Zengel, J.; Deckman, H. W.Separation of carbon dioxide from nitrogen utilizing zeolitic imidazolate framework materials. Patent no. US 20090214407. *Google Patents*, 2012.
(49) Mason, J. A.; Sumida, K.; Herm, Z. R.; Krishna, R.; Long, J. R. Evaluating Metal-Organic Frameworks for Post-Combustion Carbon Dioxide Capture via Temperature Swing Adsorption. *Energy Environ. Sci.* **2011**, *4*, 3030−40.
(50) Wu, H.; Yao, K.; Zhu, Y.; Li, B.; Shi, Z.; Krishna, R.; et al. Cu-TDPAT, an rht-type Dual-Functional Metal−Organic Framework Offering Significant Potential for Use in H2 and Natural Gas Purification Processes Operating at High Pressures. *J. Phys. Chem. C* **2012**, *116*, 16609−18.
(51) Krishna, R.; van Baten, J. M. Investigating the Relative Influences of Molecular Dimensions and Binding Energies on

DOI: 10.1021/acs.est.5b01652
Environ. Sci. Technol. 2015, 49, 9364−9373

Diffusivities of Guest Species Inside Nanoporous Crystalline Materials. *J. Phys. Chem. C* **2012**, *116*, 23556−68.
(52) Krishna, R.; van Baten, J. M. Investigating the Influence of Diffusional Coupling on Mixture Permeation across Porous Membranes. *J. Membr. Sci.* **2013**, *430*, 113−28.
(53) Ruthven, D.M.; Farooq, S.; Knaebel, K.S. *Pressure Swing Adsorption*; VCH Publishers, New York, 1994.
(54) Bao, Z.; Alnemrat, S.; Yu, L.; Vasiliev, I.; Ren, Q.; Lu, X.; et al. Kinetic separation of carbon dioxide and methane on a copper metal−organic framework. *J. Colloid Interface Sci.* **2011**, *357* (2), 504−9.
(55) Krishna, R.; Long, J. R. Screening Metal-Organic Frameworks by Analysis of Transient Breakthrough of Gas Mixtures in a Fixed Bed Adsorber. *J. Phys. Chem. C* **2011**, *115* (26), 12941−50.
(56) Krishna, R. The Maxwell-Stefan description of mixture diffusion in nanoporous crystalline materials. *Microporous Mesoporous Mater.* **2014**, *185*, 30−50.
(57) He, Y. B.; Krishna, R.; Chen, B. L. Metal-organic frameworks with potential for energy-efficient adsorptive separation of light hydrocarbons. *Energy Environ. Sci.* **2012**, *5* (10), 9107−20.
(58) Wu, X.; Niknam Shahrak, M.; Yuan, B.; Deng, S. Synthesis and characterization of zeolitic imidazolate framework ZIF-7 for CO2 and CH4 separation. *Microporous Mesoporous Mater.* **2014**, *190* (0), 189−96.
(59) Reyes, S. C.; Ni, Z.; Paur, C. S.; Kortunov, P.; Zengel, J.; Deckman, H. W.Separation of carbon dioxide from nitrogen utilizing zeolitic imidazolate framework materials. Patent no. US 20090214407 A1. 2012.

DOI: 10.1021/acs.est.5b01652
Environ. Sci. Technol. 2015, 49, 9364−9373

Supporting Material

Hydroquinone and Quinone-grafted Porous Activated Carbons for Highly Selective CO_2 Capture from Flue Gases and Natural Gas Upgrading

Jun Wang [a], Rajamani Krishna [b], Jiangfeng Yang [c], Shugaung Deng [a *]

[a.] Chemical Engineering Department,

New Mexico State University,

Las Cruces, New Mexico,88003, USA

[b.] Van't Hoff Institute for Molecular Sciences,

University of Amsterdam,

Science Park 904, 1098 XH Amsterdam, The Netherlands

[c.] Research Institute of Special Chemicals,

Taiyuan University of Technology,

Taiyuan 030024, Shanxi, PR China

*Corresponding author: Tel: +1-575-646-4346; Fax: +1-575-646-7706.

-E-mail address: sdeng@nmsu.edu

Table of Contents

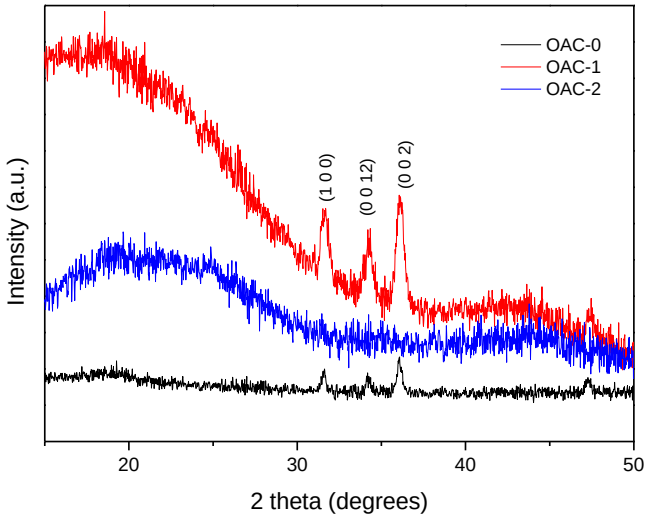

Figure S1. XRD patterns of OAC-1, OAC-1 and OAC-2.

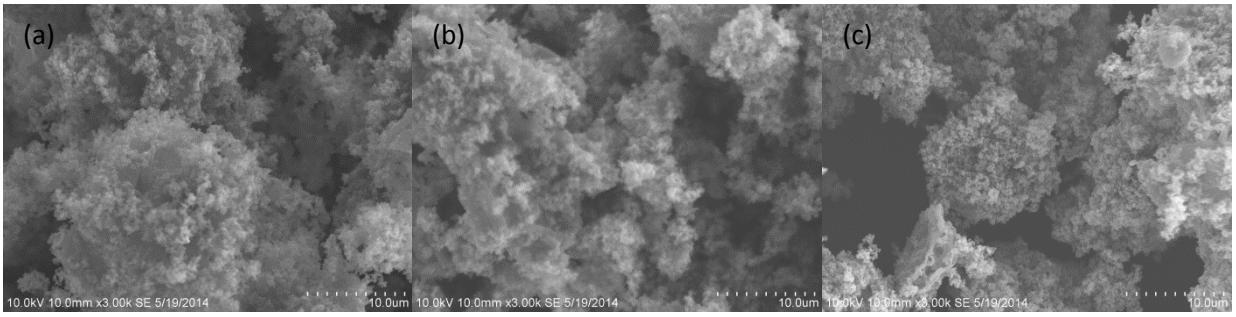

Figure S2. Representative SEM images of the a) OAC-1, b) OAC-1 and c) OAC-2 showing the similarity in the pore structure of the carbon pre- and post-modification.

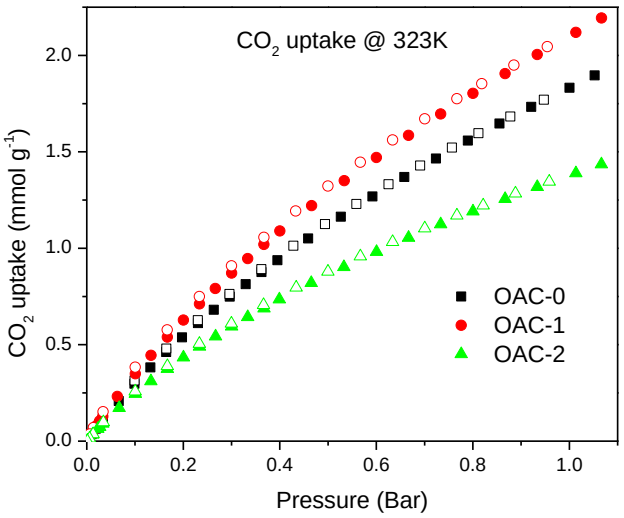

Figure S3. CO_2 adsorption 323K of OAC-0, OAC-1, and OAC-2.

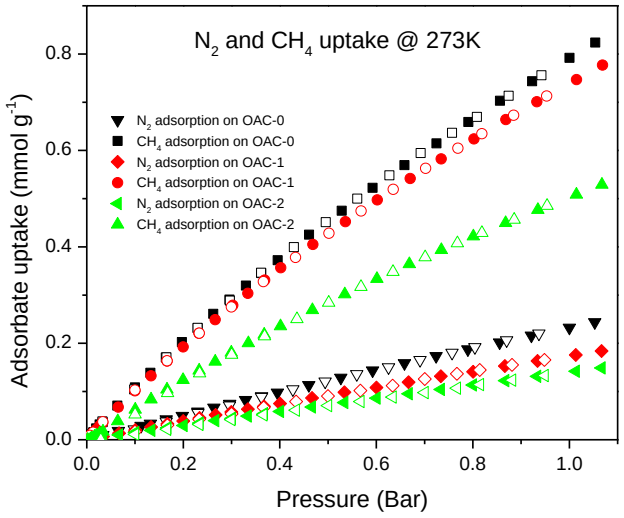

Figure S4. (a) CH_4 and N_2 adsorption 323K of OAC-0, OAC-1, and OAC-2.

Fitting of pure component isotherms

The experimentally measured loadings for (a) CO_2, (b) CH_4, and (c) N_2 were measured as a function of the absolute pressure at three different temperatures 273 K, 298 K, and 323 K.

The isotherm data for all three guest molecules in OAC-0, OAC-1, and OAC-2 were fitted with the Langmuir model

$$q = q_{sat}\frac{bp}{1+bp} \tag{1}$$

with T-dependent parameter b

$$b = b_0 \exp\left(\frac{E}{RT}\right) \tag{2}$$

The Langmuir fit parameters are provided in Table S1, Table S2, and Table S3.

Table S5. 1-site Langmuir parameters for adsorption of CO_2 in different OACs.

	q_{sat} mol kg^{-1}	b_0 Pa^{-1}	E kJ mol^{-1}
OAC-0	6.7	5.5×10^{-10}	23.8
OAC-1	7.6	6.34×10^{-10}	23.5
OAC-2	4.8	8.16×10^{-10}	23

Table S6. 1-site Langmuir parameters for CH_4 in different OACs.

	q_{sat} mol kg^{-1}	b_0 Pa^{-1}	E kJ mol^{-1}
OAC-0	3.75	1.67×10^{-9}	19.8
OAC-1	3	2.11×10^{-9}	20
OAC-2	2.5	1.802×10^{-9}	20.9

Table S7. 1-site Langmuir parameters for N_2 in different OACs.

	q_{sat} mol kg^{-1}	b_0 Pa^{-1}	E kJ mol^{-1}
OAC-0	3.1	2.08×10^{-9}	16
OAC-1	2.9	4.18×10^{-10}	19.6
OAC-2	2.3	6.65×10^{-10}	18.4

IAST calculations

The adsorption selectivity for the mixtures CH_4/N_2 and CO_2/CH_4 defined by

$$S_{ads} = \frac{q_1/q_2}{p_1/p_2}$$

were calculated according to IAST model proposed by Myers [1,2]. In above equation, q_1 and q_2 are the absolute component loadings of the adsorbed phase in the mixture. These component loadings are also termed the uptake capacities.

Isosteric heat of adsorption

The isosteric heat of adsorption, Q_{st}, defined as

$$Q_{st} = RT^2\left(\frac{\partial \ln p}{\partial T}\right)_q$$

were determined using the pure component isotherm fits using the Clausius-Clapeyron equation, where Qst (kJ/mol) is the isosteric heat of adsorption, T (K) is the temperature, p (kPa) is the pressure, R is the gas constant. The values of Q_{st} for CO_2, CH_4, and N_2 are provided in Table S4 of OACs.

Table S8. Isosteric heats of adsorption of CO_2, CH_4 and N_2 in different OACs.

	Q_{st}, CO_2 kJ mol^{-1}	Q_{st}, CH_4 kJ mol^{-1}	Q_{st}, N_2 kJ mol^{-1}
OAC-0	23.8	19.8	16
OAC-1	23.5	20	19.6
OAC-2	23	20.9	18.4

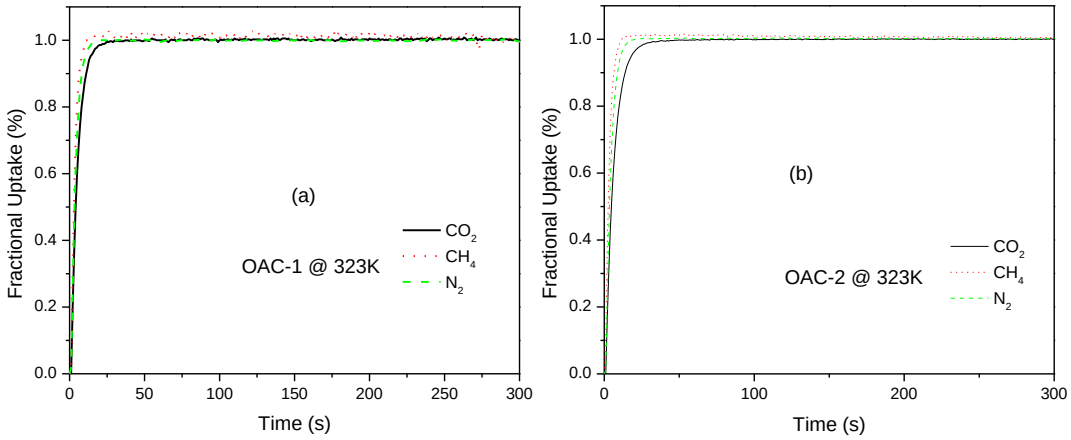

Figure S5. CO_2, CH_4, and N_2 fractional uptake on (a) OAC-1, (b) OAC-2 at 323 K.

Table S5. Summary of Diffusion Time Constants of CO_2, CH_4, and N_2 on the OACs at 323 K.

Sample	CO_2 D_c/r^2_c (10^{-3} s^{-1})	CH_4 D_c/r^2_c (10^{-2} s^{-1})	N_2 D_c/r^2_c (10^{-3} s^{-1})
OAC-1	7.5	1.9	8.1
OAC-2	8.2	1.1	7.4

Simulation methodology for transient breakthrough in fixed bed adsorbers

The separation of CO_2/CH_4, CO_2/N_2, and CH_4/N_2 mixtures is commonly carried out in fixed bed adsorbers in which the separation performance is dictated by a combination of three separate factors: (a) adsorption selectivity, (b) uptake capacity, and (c) intra-crystalline diffusivities of guest molecules within the pores. Transient breakthrough simulations are required for a proper evaluation of microporous materials; the simulation methodology used in our work is described in earlier publications [3,4].

In order to evaluate the different OACs, breakthrough calculations were performed taking the following parameter values: inside diameter of tube = 50 mm; bed length, L = 1.8 m; voidage of bed, ε = 0.5; superficial gas velocity, u = 0.05 m/s (at inlet), interstitial velocity, v = 0.1 m/s. The mass of adsorbent packed in the tube is 2 kg; see schematic in Figure S6.

A brief summary of the simulation methodology is presented below.Assuming plug flow of an n-component gas mixture through a fixed bed maintained under isothermal conditions (see schematic in Figure **0**), the partial pressures in the gas phase at any position and instant of time are obtained by solving the following set of partial differential equations for each of the species i in the gas mixture [5].

$$\frac{1}{RT}\frac{\partial p_i(t,z)}{\partial t} = -\frac{1}{RT}\frac{\partial\left(v(t,z)\,p_i(t,z)\right)}{\partial z} - \frac{(1-\varepsilon)}{\varepsilon}\rho\frac{\partial \bar{q}_i(t,z)}{\partial t}; \quad i = 1,2,...n \tag{1}$$

In equation (1), t is the time, z is the distance along the adsorber, ρ is the framework density, ε is the bed voidage, v is the interstitial gas velocity, and $\bar{q}_i(t,z)$ is the *spatially averaged* molar loading within the crystallites of radius r_c, monitored at position z, and at time t.

At any time t, during the transient approach to thermodynamic equilibrium, the spatially averaged molar loading within the crystallite r_c is obtained by integration of the radial loading profile

$$\bar{q}_i(t) = \frac{3}{r_c^3}\int_0^{r_c} q_i(r,t)r^2 dr \tag{2}$$

For transient unary uptake within a crystal at any position and time with the fixed bed, the radial distribution of molar loadings, q_i, within a spherical crystallite, of radius r_c, is obtained from a solution of a set of differential equations describing the uptake

$$\frac{\partial q_i(r,t)}{\partial t} = -\frac{1}{\rho}\frac{1}{r^2}\frac{\partial}{\partial r}\left(r^2 N_i\right) \tag{3}$$

The molar flux N_i of component i is described by the simplified version of the Maxwell-Stefan equations in which both correlation effects and thermodynamic coupling effects are considered to be of negligible importance [4]

$$N_i = -\rho Đ_i\frac{\partial q_i}{\partial r} \tag{4}$$

Summing equation (2) over all n species in the mixture allows calculation of the *total average* molar loading of the mixture within the crystallite

$$\bar{q}_t(t,z) = \sum_{i=1}^{n} \bar{q}_i(t,z) \tag{5}$$

The *interstitial* gas velocity is related to the *superficial* gas velocity by

$$v = \frac{u}{\varepsilon} \tag{6}$$

In industrial practice, the most common operation uses a step-wise input of mixtures to be separated into an adsorber bed that is initially free of adsorbates, i.e. we have the initial condition

$$t = 0; \quad q_i(0,z) = 0 \tag{7}$$

At time, $t = 0$, the inlet to the adsorber, $z = 0$, is subjected to a step input of the n-component gas mixture and this step input is maintained till the end of the adsorption cycle when steady-state conditions are reached.

$$t \geq 0; \quad p_i(0,t) = p_{i0}; \quad u(0,t) = u_0 \tag{8}$$

where u_0 is the superficial gas velocity at the inlet to the adsorber.

The breakthrough characteristics for any component is essentially dictated by two sets of parameters: (a) The characteristic contact time $\frac{L}{v} = \frac{L\varepsilon}{u}$ between the crystallites and the surrounding fluid phase, and (b) $\frac{Đ_i}{r_c^2}$, that reflect the importance of intra-crystalline diffusion limitations. It is common to use the dimensionless time, $\tau = \frac{tu}{L\varepsilon}$, obtained by dividing the actual time, t, by the characteristic time, $\frac{L\varepsilon}{u}$ when plotting simulated breakthrough curves [3].

If the value of $\frac{Đ_i}{r_c^2}$ is large enough to ensure that intra-crystalline gradients are absent and the entire crystallite particle can be considered to be in thermodynamic equilibrium with the surrounding bulk gas phase at that time *t*, and position *z* of the adsorber

$$\bar{q}_i(t,z) = q_i(t,z) \tag{9}$$

The molar loadings at the *outer surface* of the crystallites, i.e. at $r = r_c$, are calculated on the basis of adsorption equilibrium with the bulk gas phase partial pressures p_i at that position *z* and time *t*. The adsorption equilibrium can be calculated on the basis of the IAST. The assumption of thermodynamic equilibrium at every position *z*, and any time *t*, i.e. invoking Equation (5), generally results in sharp breakthroughs for each component. Sharp breakthroughs are desirable in practice because this would result in high productivity of pure products. Essentially, the influence of intra-crystalline diffusion is to reduce the productivity of pure gases. For all the breakthrough calculations reported in this work, we assume negligible diffusion resistances for all materials and we invoke the simplified Equation (5).

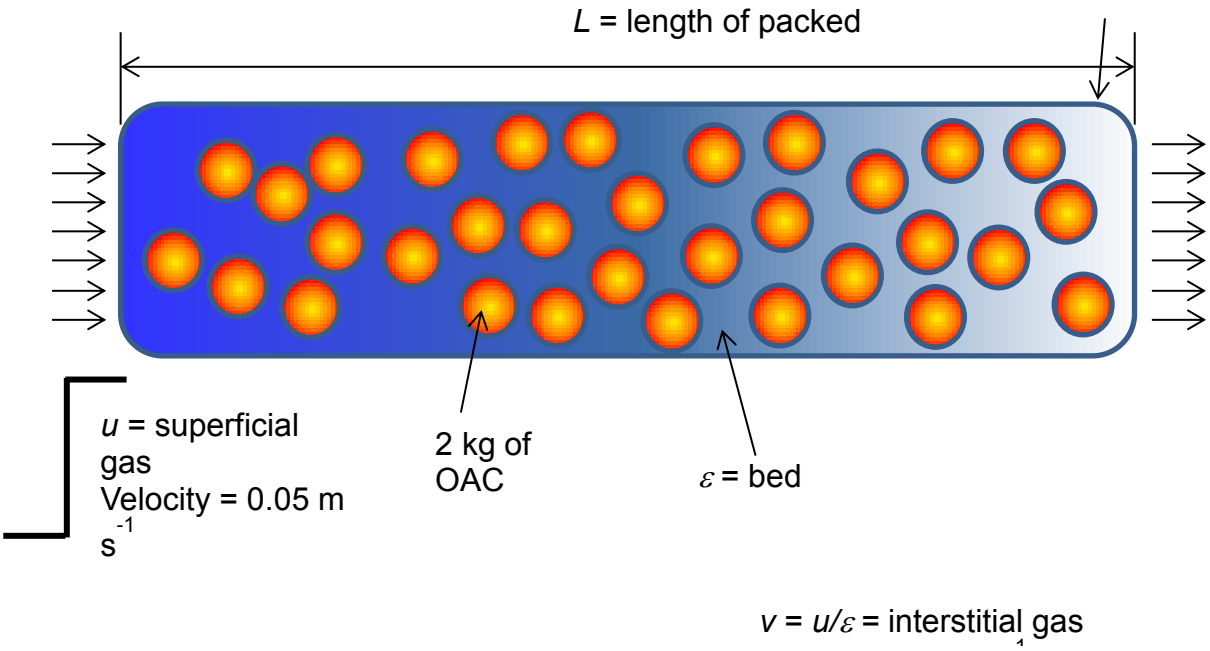

Figure S6. Schematic of the breakthrough apparatus.

Notation

b	Langmuir-Freundlich constant for species i at adsorption site A, $\mathrm{Pa}^{-\nu_i}$
c_i	molar concentration of species i in gas mixture, mol m^{-3}
c_{i0}	molar concentration of species i in gas mixture at inlet to adsorber, $molm^{-3}$
E	energy parameter, J mol^{-1}
L	length of packed bed adsorber, m
N_i	molar flux of species i, mol m^{-2} s^{-1}
p_i	partial pressure of species i in mixture, Pa
p_t	total system pressure, Pa
q_i	component molar loading of species i, mol kg^{-1}
$\bar{q}_i(t)$	spatially averaged component molar loading of species i, mol kg^{-1}
Q_{st}	isosteric heat of adsorption, J mol^{-1}
r_c	radius of crystallite, m
R	gas constant, 8.314 J mol^{-1} K^{-1}
t	time, s
T	absolute temperature, K
u	superficial gas velocity in packed bed, m s^{-1}
v	interstitial gas velocity in packed bed, m s^{-1}

Greek letters

ε	voidage of packed bed, dimensionless
ρ	framework density, kg m^{-3}
τ	time, dimensionless

Reference

[1]. Myers, A. L.; Prausnitz, J. M. Thermodynamics of mixed gas adsorption, A.I.Ch.E.J. 1965, 11, 121-130.

[2]. Myers AL. Equation of state for adsorption of gases and their mixtures in porous materials. Adsorption. 2003 Mar;9(1):9-16.

[3]. Krishna R, Long JR. Screening metal-organic frameworks by analysis of transient breakthrough of gas mixtures in a fixed bed adsorber. J Phys Chem C. 2011;115:12941-50.

[4]. Krishna R. The Maxwell-Stefan Description of Mixture Diffusion in Nanoporous Crystalline Materials. Microporous Mesoporous Mater. 2014;185:30-50.

[5]. Krishna R, Baur R. Modelling issues in zeolite based separation processes. Sep Purif Technol. 2003;33:213-54.